Acta Scientific PAEDIATRICS (ISSN: 2581-883X)

Volume 3 Issue 8 August 2020

Review Article

An Electron-based Paediatric Pulmonary Magnetic Resonance Imaging Device to Avoid Administering General Anaesthesia to Paediatric Patients while being Imaged by Exploiting the 'Celalettin Tunnel Conjecture'

Metin Celalettin[1]* and Horace King[2]

[1]*TEPS, Victoria University, Australia*

[2]*College of Engineering and Science, Victoria University, Australia*

***Corresponding Author:** Metin Celalettin, TEPS, Victoria University, Australia.

Received: June 26, 2020

Published: July 30, 2020

Abstract

The 'Celalettin-Field Quantum Observation Tunnel' (Celalettin Tunnel) is a quantum observation technique. It is within a pneumatic manifold of Euclidean space where the randomness of particle Orbital Angular Momentum (OAM) is mitigated via electric polarization. It is described by the Celalettin Tunnel Conjecture: The presence of an electric field affects the nuclear spin of the particles within the pneumatic manifold. The manifold, namely the IC-Manifold, or Invizicloud© is unique as its axioms are a combination of classical and quantum non-logical parameters. The IC-Manifold has a variable density and exists only according to 'Celalettin's two rules of quantum interaction:

- Quantum interaction causes quantum observation during fundamental particle interactions with orbital angular momentum electric polarized atoms within the IC-Manifold causing depolarization.
- The photoelectric effect is not limited to solids but can occur in an IC-Manifold.

The 'Celalettin Tunnel Conjecture' can be exploited to make proposals to 'Magnetic Resonance Imaging (MRI) machines, such that it could develop an MRI for paediatric use. Paediatric patients are typically administered a General Anaesthesia when undergoing MRI imaging due to the requirement to stay still for extended periods. MRI developed from NMR uses the same phenomena to identify chemical structures based on a spectrum. A technique; *in vivo* MR spectrograph allows chemical identification on specific parts of the brain. Looking at whether the cells in a brain tumour contain alpha-hydroxy glutaric acid differentiates gliomas that have a mutation in the IDH1 or IDH2 gene for example. Pulse sequences to glean biochemical information non-invasively can be recalibrated for different patients.

In an MRI, the flip angle is the rotation of the nuclear spin vector relative to the main magnetic field. To improve the signal with an MRI, the flip angle needs to be chosen using the Ernst angle. A 90° flip angle using the Ernst angle will yield the maximum signal intensity (or signal-to-noise ratio) per number of averaged Free Induction Decays (FID)s. The flips are done over and over against while the patient stays still, and the average number of nuclear spin ensembles is taken to produce the image. This can involve the patient remaining still for up to five minutes.

This study explores a 180° flip angle could be achieved, then rather than taking several measurements over the five-minute imaging time experienced by the patient, it could produce a decisive image one measurement. The way to do this would be to focus on the electron rather than the proton. Free electrons are not only aligned with a magnetic field but can be manipulated to be pulled into the direction of the south pole.

Keywords: Celalettin Tunnel; Magnetic Resonance; Anaesthesia

Introduction

The brain is surrounded by cerebrospinal fluid (CSF), which has roughly the same signal intensity on images as brain tissue. So there a pulse sequence called (fluid attenuation inversion recovery) FLAIR that makes hyperintense signals from water turn hypointense (black) on T2 images while keeping lesions hyperintense and recognisable [11]. This is the same as other tissues in the body; their FLAIR signals are too similar for a single quarter-second image, so multiple investigative techniques are required by the MRI to produce images [10,11]. This weakness in extant MRI technologies causes paediatric patients to be administered a general anaesthesia; a risk that medical practitioners claim outweighs the benefits of diagnostic techniques without an MRI [11,12].

Celalettin tunnel: The technique

Anti-ferromagnetism affects the OAM spin within the pneumatic matter inside the IC-Manifold [1,2].

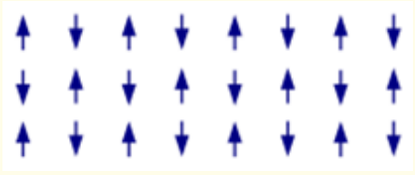

Figure 1: Antiferromagnetic ordering.

The Celalettin Tunnel theoretically works similarly to magnetic resonance imaging [3,4]. An entangled photon depolarizes Helium-3 atoms as it burrows through the IC-Manifold and creates a tunnel [5]. The depolarized particles are considered a single quantum system and can be used to acquire information on the signaller [5-9]. The photon would become weaker as it scattered through an ensemble of atomic Helium-3 until it was absorbed or escaped [10-12].

Figure 2: Celalettin-Field quantum observation tunnel in an IC-Manifold (Helium-3 atoms in grey have been depolarized).

At figure 2, the Celalettin Tunnel is made from the collective depolarized electrons in the IC-Manifold after the signaller has penetrated it [3,5,13,14]. Immediately after the signaller produced a tunnel through the IC-Manifold [5,9,15,16]. If a gas is subject to anti-ferromagnetism its intrinsic spin properties will polarize and portray entropy attributes such like a solid [4,17,18]. Those affected atoms could emit a bound electron depending on the photon's energy, given:

$$\frac{n_{i+1}n_e}{n_i} = \frac{2}{\lambda^3}\frac{g_{i+1}}{g_i}\exp\left[-\frac{(\epsilon_{i+1}-\epsilon_i)}{k_BT}\right] \quad \text{---------- (1)}$$

Where:

n_i = The density of atoms in the i-th state of ionization, that is with i electrons removed.

g_i = The degeneracy of states for the i-ions.

ϵ_i = The energy required to remove i electrons from a neutral atom, creating an i-level ion.

n_e = Is the electron density.

λ = The thermal de Broglie wavelength of an electron.

We use the classical models by considering the classical spins with magnetic moments μA 6= μB. To simplify we assume that nuclear spin interaction is disordered of the Heisenberg form [9,22,23,27]. So, the ferromagnet model described by the classical Hamiltonian of the type:

$$\langle \zeta_{i,\alpha}(t)\zeta_{j,\beta}(t')\rangle = \frac{2\lambda_i k_B T}{\mu_i \gamma_i}\delta_{ij}\delta_{\alpha\beta}\delta(t-t') \quad \text{----------(2)}$$

$$H_{i,tot} \equiv -\frac{1}{\mu_i}\frac{\partial \mathcal{H}}{\partial s_i} = H + \frac{2D_i}{\mu_i}s_i^z e_z + \frac{1}{\mu_i}\sum_{j\in neig(i)} J_{ij}s_{ij} \quad \text{----------(3)}$$

Where:

H = Hamiltonian

N = Total number of spins

I and J = Lattice sites

D_i = The anisotropy constant of site I

$|S_i| = 1$ The third sum is over neighbour pairs

J_{ij} = JAA(BB)>0 Heisenberg exchange interaction parameter

λ_i = Is the coupling to the heat bath parameter

a,B = Cartesian Z components heat bath and T is the temperature.

Each point of an n-dimensional manifold has a neighbourhood or a set of points acting like barriers, defining the region where the content within the IC-Manifold can exist, or the walls of the IC-Manifold itself [17] [24]. Helium-3 has an intrinsic nuclear spin of ½ and can be hyperpolarized by spin exchange optical pumping. Depolarization occurs to make way for the quantum entangled

photon [4]. Hyperpolarization using non-equilibrium means for spin-exchange optical pumping is achieved by Coulomb Forces; such that:

$$F = \frac{1}{4\pi\varepsilon_0}\frac{qQ}{r^2} = k_0\frac{qQ}{r^2} \quad \text{----------(4)}$$

Where:

r = The distance between the two charges q and Q Newtons.

Given the Boltzmann equation to accommodate the density of the environment in which the photon-electron interactions will occur in the presence of an electric field:

$$n_e(\phi_2) = n_e(\phi_1)e^{e(\phi_2-\phi_1)/k_BT_e} \quad \text{----------(5)}$$

Where:

n_e = Electron number density

T_e = Temperature of the plasma, and

k_B = Boltzmann constant.

φ = Work function.

Fluid attenuation inversion recovery in paediatric 'Severe Acute Respiratory Syndrome Coronavirus-2' (COVID-19) patients.

MRI developed from NMR uses the same phenomena to identify chemical structures based on a spectrum [1,2,11]. A technique; *in vivo* MR spectrograph allows chemical identification on specific parts of the brain. Looking at whether the cells in a brain tumour contain alpha-hydroxy glutaric acid differentiates gliomas that have a mutation in the IDH1 or IDH2 gene for example. Pulse sequences to glean biochemical information non-invasively can be recalibrated for different patients [11,12].

In an MRI, the flip angle is the rotation of the nuclear spin vector relative to the main magnetic field. To improve the signal with an MRI, the flip angle needs to be chosen using the Ernst angle:

$$\cos(\theta_E) = e^{-(d_1+a_t)/T_1} \quad \text{----------(6)}$$

A 90° flip angle using the Ernst angle will yield the maximum signal intensity (or signal-to-noise ratio) per number of averaged Free Induction Decays (FID)s. The flips are done over and over against while the patient stays still, and the average number of nuclear spin ensembles is taken to produce the image [1,2,11]. This can involve the patient remaining still for up to five minutes.

If a 180° flip angle could be achieved, then rather than taking several measurements over the five-minute imaging time experienced by the patient, it could produce a decisive image one measurement. The way to do this would be to focus on the electron rather than the proton. Free electrons are not only aligned with a magnetic field but can be manipulated to be pulled into the direction of the south pole [11,12].

Increasing the flip angle parameter by exploiting the celalettin tunnel conjecture

If the electron were pulled at a 180° flip angle in an MRI, then the patient would be exposed to a length of time of imaging in the diagnostic of 'Severe Acute Respiratory Syndrome Coronavirus-2' comparable to a handheld ultrasound or a CT. The electromagnetic strength required is given by Faraday's law of induction. The trajectory of an ensemble of particles is derived from the Lagrange equations, where the Euler-Lagrange equation describes the motion for the scalar field [1].

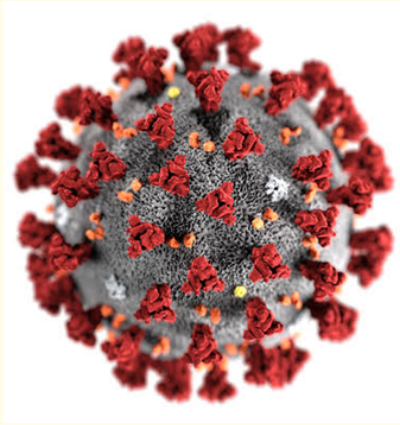

Figure 3: 'Severe Acute Respiratory Syndrome Coronavirus-2' (COVID-19).

A paediatric patient suffering 'Severe Acute Respiratory Syndrome Coronavirus-2' (COVID-19). It infects and damages the type II alveolar cells of the lungs. Common symptoms include fever, cough, and shortness of breath. While chest CT is considered the modality of choice to diagnose pulmonary damage, such scans aren't always as conclusive as an MRI [11].

As an alternative, bedside lung ultrasound is frequently used as a diagnostic. As the global infection rates of COVID-19 continue to

rise, investigators in Italy evaluated whether lung ultrasound could be an effective tool in also identifying patients who have pneumonia specifically associated with the virus. The results weren't significant. However, since its inception, the MRI has been the Rolls Royce of diagnostic imaging [3-5,11,12].

For an adult, it would be unlikely that they would need an MRI as a CT scan would be sufficient, however in a paediatric patient where complications of Covid-19, pneumonia and other respiratory conditions, it may be too difficult to use these techniques. To determine whether ultrasound could feasibly be used to pinpoint COVID-19 pneumonia, researchers analysed 12 emergency department patients with the COVID-19 infection. These individuals received both lung ultrasound and CT. CT scans correlated strongly with the ultrasounds. 12 patients had ground-glass opacity; five patients had a crazy-paving pattern. Scans identified a diffuse B-pattern with spared areas in all patients, and only three had posterior subpleural consolidations. The research showed that using a hand-held ultrasound was about as effective as a CT scan, where in the past, CT scans were the standard protocol for COVID-19 diagnostics.

Celalettin tunnel: The conjecture

In an IC-Manifold, the Celalettin Tunnel is theoretically produced by an incoming entangled photon. When viewed as a single quantum system, the collectively affected Helium-3 atoms describe the photon.

The Schrodinger wave function equation:

$$\nabla^2\Psi+\frac{8\pi^2 m}{h^2}(E-V)\,\Psi=0 \qquad \text{----------(7)}$$

Where the Laplacian of a scalar for spherical coordinates is given by:

$$\Delta f=\frac{1}{r^2}\frac{\partial}{\partial r}\left(r^2\frac{\partial f}{\partial r}\right)+\frac{1}{r^2\sin\theta}\frac{\partial}{\partial\theta}\left(\sin\theta\frac{\partial f}{\partial\theta}\right)+\frac{1}{r^2\sin^2\theta}\frac{\partial^2 f}{\partial\varphi^2}$$
$$=\frac{1}{r}\frac{\partial^2}{\partial r^2}(rf)+\frac{1}{r^2\sin\theta}\frac{\partial}{\partial\theta}\left(\sin\theta\frac{\partial f}{\partial\theta}\right)+\frac{1}{r^2\sin^2\theta}\frac{\partial^2 f}{\partial\varphi^2} \qquad \text{----------(8)}$$

Where:

E = Energy

V = Potential Energy

m = Mass

h = Planck's constant

φ = The azimuthal angle, and

θ = The zenith angle or co-latitude.

Rearranged to express quantum entangled photons:

$$|\Psi\rangle=\frac{1}{\sqrt{2}}(|e,\alpha e^{i\phi}\rangle+|g,\alpha e^{-i\phi}\rangle) \qquad \text{----------(9)}$$

Where:

αe = Eigenvalues

e = γ_{sig}

g = γ_{idler}.

Bra-ket notation

An electron's spin: |↑|↑

With an observer: |↑|obs|↑|obs

For an entangled quantum system: |↑⟹(|→+|←)/2–√|↑⟹(|→+|←)/2

Where the observer is added: |↑|obs⟹(|→+|←)|obs/2–√|↑|obs⟹(|→+|←)|obs/2.

If the observer can measure the state, then the state of the observer changes and the observer can no longer be factored out of the whole state: (|→|obs1+|←|obs2)/2–√(|→|obs1+|←|obs2)/2. The quantumness of |obs1≠|obs2|obs1≠|obs2 describes the electron spin as not acting quantum mechanically and hence decoherence is achieved [25].

Spin exchange optical pumping can be represented by:

$$P_N(t)=\langle P_A\rangle\left(\frac{\gamma_{SE}}{\gamma_{SE}+\Gamma}\right)[1-e^{(\gamma_{SE}+\Gamma)t}] \qquad \text{----------(10)}$$

Where:

$P_N(t)$ = Nuclear polarization (spin)

(P_A) is the atom's polarization

γ_{SE} = The spin exchange rate

Γ = The longitudinal relaxation rate.

The Lagrangian scalar formulation to investigate the required kinetic energy of a photon to cause the Celalettin Tunnel [24]. It is given by:

$$\mathcal{L}_{sQED}=\frac{1}{2}\left[\left(\partial_\mu+ieA_\mu\right)\Phi^*\right]\left[\left(\partial^\mu-ieA^\mu\right)\Phi\right]$$
$$-\frac{1}{2}M^2\Phi*\Phi-\frac{1}{16\pi}F_{\mu\nu}F^{\mu\nu} \qquad \text{----------(11)}$$

Where:

Φ = Charged scalar field,

Φ∗ = Its complex conjugate.

The electromagnetic strength required is given by Faraday's law of induction. The trajectory of an ensemble of particles is derived from the Lagrange equations, where the Euler-Lagrange equation describes the motion for the scalar field [1]:

$$\frac{\delta \mathcal{L}}{\delta \Phi *} = \partial_\mu \frac{\delta \mathcal{L}}{\delta \left(\partial_\mu \Phi *\right)} \quad \text{----------(12)}$$

Yielding the Klein-Gordon [15]

$$\left[-\partial^2 + M^2\right]\Phi = \left[-e^2 A^2 + 2ieA \cdot \partial\right]\Phi \quad \text{----------(13)}$$

Where:

$\partial^2 \equiv \partial\mu\partial\mu$,

$A^2 \equiv A\mu A\mu$

$A \cdot \partial \equiv A\mu\partial\mu$

Further,

$$\frac{d^2y}{dx^2} + (a - 2q\cos 2x)y = 0 \quad \text{----------(14)}$$

Where:

a and q are the quantum parameters.

That is repolarizing the Celalettin Tunnel within the IC-Manifold. That time is expected to occur, given:

$$M_{xy}(t) = M_{xy}(0)e^{-t/T_2} \quad \text{----------(15)}$$

Where:

M_{xy}= the transverse component of the magnetization vector

T_2= a time constant characterizing the signal decay

e = Euler's number.

A 'Celalettin Tunnel Conjecture' can therefore mathematically be described:

$$T_{\text{Celalettin}} = \Psi, Ce_n, \mathcal{L}_{QED}, P_N(t) \quad \text{----------(16)}$$

Where:

$T_{Celalettin}$ is the Celalettin Tunnel

- is the Schrodinger equation

Ce_n is the Mathieu differential equation

$\mathcal{L}_{QED}$ symbolizes Lagrangian QED

$P_N(t)$ is the rate of nuclear spin repolarization.

Conclusion

While the Celalettin Tunnel Conjecture exploits antiferromagnetism to manipulate particle spin, it can be used on free electrons in paediatric patients, and if pulled at a 180° flip angle in an MRI, then the patient could be exposed to a length of time of imaging in the diagnostic of 'Severe Acute Respiratory Syndrome Coronavirus-2' comparable to a handheld ultrasound or a CT. This would avoid the need to administer General Anesthesia to paediatric patients undergoing pulmonary imaging for COVID-19 diagnostics.

Bibliography

1. E Raicher., *et al*. "The Lagrangian formulation of strong-field quantum electrodynamics in a plasma". *Physics of Plasmas* 21.5 (2014): 053103.

2. M Lanzagorta. "Quantum radar". *Synthesis Lectures on Quantum Computing* 3.1 (2011): 1-139.

3. Salerno M., *et al*. "Emphysema: hyperpolarized helium 3 diffusion MR imaging of the lungs compared with spirometric indexes—initial experience". *Radiology* 222.1 (2002): 252-260.

4. Walker TG and Happer W. "Spin-exchange optical pumping of noble-gas nuclei". *Reviews of Modern Physics* 69.2 (1997): 629.

5. Celalettin M and King H. "The 'Celalettin-Field Quantum Observation Tunnel'; a Quantum Communication Countermeasure Speculative Structure". *Scholar Journal of Applied Sciences and Research* 1.9 (2009): 5-9.

6. Bassi K., *et al*. "Models of wave-function collapse, underlying theories, and experimental tests". *Reviews of Modern Physics* 85.2 (2013): 471.

7. Gaëtan., *et al*. "Observation of collective excitation of two individual atoms in the Rydberg blockade regime". *Nature Physics* 5.2 (2009): 115.

8. WH Zurek. "Decoherence and the transition from quantum to classical—revisited". in Quantum Decoherence: Springer (2006): 1-31.

9. W. Heisenberg. "Über den anschaulichen Inhalt der quantentheoretischen Kinematik und Mechanik". in Original Scientific Papers Wissenschaftliche Originalarbeiten: Springer (1985): 478-504.

10. P Christillin. "Nuclear Compton scattering". *Journal of Physics G: Nuclear and Particle Physics* 12.9 (2006): 837-851.

11. Joos HD Zeh., *et al*. "Decoherence and the appearance of a classical world in quantum theory". Springer Science and Business Media (2013).

12. Singh S., *et al*. "Plasma-based radar cross section reduction". in Plasma-based Radar Cross Section Reduction: Springer (2016): 1-46.

13. Stewart J. "Angular momentum of the electromagnetic field: the plane wave paradox resolved". *European Journal of Physics* 26.4 (2005): 635.

14. Fox. An introduction to the calculus of variations. Courier Corporation (1987).

15. E Raicher., *et al*. "A novel solution to the Klein–Gordon equation in the presence of a strong rotating electric field". *Physics Letters* B 750 (2015): 76-81.

16. Heisenberg W and Bond B. "Physics and philosophy: the revolution in modern science". St. Leonards, Australia: Allen and Unwin (1959).

17. Gachet D., *et al*. "Revisiting the Young's double slit experiment for background-free nonlinear Raman spectroscopy and microscopy". *Physical Review Letters* 104.21 (2010): 213905.

18. H Shirley. "Solution of the Schrödinger equation with a Hamiltonian periodic in time". *Physical Review* 138.4B (1965): B979.

19. Marrucci C Manzo and D Paparo. "Optical spin-to-orbital angular momentum conversion in inhomogeneous anisotropic media". *Physical Review Letters* 96.16 (2006): 163905.

20. Lüdge K and Finley JJ. "Long-term mutual phase locking of picosecond pulse pairs generated by a semiconductor nanowire laser". *Nature Communications* 8 (2017): 15521.EH Allen.

21. M Forrester and F Kusmartsev. "The nano-mechanics and magnetic properties of high moment synthetic antiferromagnetic particles". *Physica Status Solidi A* 211.4 (2014): 884–889.

22. Kimichika Fukushima. "Electronic Structure Calculations for Anti-ferromagnetism of Cuprates Using SIWB Method for Anions in DV and a Density Functional Theory Confirming from Finite Element Method". *Advances in Quantum Chemistry* 70 (2015): 1-29.

23. MJ Brandsema., *et al*. "Design considerations for quantum radar implementation". in Proc. of SPIE 9077 (2014): 90770T-1.

24. S Haroche. "Cavity Quantum Electrodynamics: a review of Rydberg atom-microwave experiments on entanglement and decoherence". in AIP Conference Proceedings 464.1 (1999): 45-66.

25. Panarella E. "Heisenberg uncertainty principle". in Annales de la Fondation Louis de Broglie 12.2 (1987): 165-193.

26. Bozorth Richard M. Ferromagnetism, first published 1951, reprinted 1993 by IEEE Press, New York as a "Classic Reissue".